Homozygous pathogenic variants in *ACTL9* cause fertilization failure and male infertility in humans and mice

Jing Dai,[1,2,3,6] Tianlei Zhang,[2,3,4,6] Jing Guo,[2,3,4] Qinwei Zhou,[2,3] Yifan Gu,[1,2,3,5] Jue Zhang,[2,3,4] Liang Hu,[1,2,3,5] Yurong Zong,[2,3] Juan Song,[2,3] Shuoping Zhang,[2,3] Can Dai,[2,3,4] Fei Gong,[1,2,3,5] Guangxiu Lu,[2,3,4,5] Wei Zheng,[2,3,4,*] and Ge Lin[1,2,3,5,*]

Summary

Total fertilization failure (TFF) can occur during *in vitro* fertilization (IVF) treatments, even following intracytoplasmic sperm injection (ICSI). Various male or female factors could contribute to TFF. Increasing evidence suggested that genetic variations in *PLCZ1*, which encodes 1-phosphatidylinositol 4,5-bisphosphate phosphodiesterase zeta-1 (PLCζ), is involved in oocyte activation and is a key male factor in TFF. In the present study, we explored the genetic variants in male individuals that led to TFF. A total of 54 couples with TFF or poor fertilization (fertilization rate < 20%) were screened, and 21 couples were determined to have a male infertility factor by the mouse oocyte activation test. Whole-exome sequencing of these 21 male individuals identified three homozygous pathogenic variants in *ACTL9* (actin like 9) in three individuals. *ACTL9* variations led to abnormal ultrastructure of the perinuclear theca (PT), and PLCζ was absent in the head and present in the neck of the mutant sperm, which contributed to failed normal calcium oscillations in oocytes and subsequent TFF. The key roles of *ACTL9* in the PT structure and TFF after ICSI were further confirmed in an *Actl9*-mutated mouse model. Furthermore, assisted oocyte activation by calcium ionophore exposure successfully overcame TFF and achieved live births in a couple with an *ACTL9* variant. These findings identified the role of *ACTL9* in the PT structure and the correct localization of PLCζ. The results also provide a genetic marker and a therapeutic option for individuals who have undergone ICSI without successful fertilization.

Introduction

Fertilization is the process by which the sperm and oocyte recognize each other, interact, and fuse to give rise to a zygote with two pronuclei (2PN).[1] One important step toward successful fertilization is the process when sperm enter the oocyte cytoplasm and release the activation factor 1-phosphatidylinositol 4,5-bisphosphate phosphodiesterase zeta-1 (PLCζ) to trigger the calcium oscillations.[2,3] Total fertilization failure (TFF), in which all mature oocytes fail to form pronuclei, is related to many factors during *in vitro* fertilization (IVF) treatments.[4,5] As reported previously, defective sperm-oocyte recognition and fusion are the chief causes of TFF after IVF.[6,7] Although intracytoplasmic sperm injection (ICSI) is able to bypass the defects in sperm-oocyte fusion, ICSI still carries a 1%–3% incidence of TFF.[8–10] In previous studies, investigators have reported that the female factors in TFF after ICSI include pathogenic variants in *WEE2* (MIM: 614084),[11] *TLE6* (MIM: 612399),[12] and *TUBB8* (MIM: 616768),[13] whereas for male factors, pathogenic variants in *PLCZ1* (MIM: 608075) were reported to be the primary cause of TFF, accounting for approximately 30% of couples with male factors involved in TFF, excluding globozoospermia.[14–19]

Rapidly accumulating evidence indicates that PLCζ, encoded by *PLCZ1*, is the key sperm-borne oocyte activation factor (SOAF).[3] PLCζ is located in the perinuclear theca (PT), a specialized structure localized under the acrosome that surrounds the nuclei of sperm heads.[20–22] Most recently, it was reported that pathogenic variants in *ACTL7A* (MIM: 604303) led to reduced expression and abnormal localization of PLCζ, thereby identifying this genetic variant as a potential cause of TFF.[23]

In the present study, we used whole-exome sequencing (WES) and identified three homozygous variants in *ACTL9* (actin like 9 [HGNC: 28494, GenBank: NM_178525.5]) in males from 21 couples suffering from TFF or poor fertilization. Our results suggest that mutant ACTL9 has weakened or lost interaction with ACTL7A that causes abnormal localization of PLCζ and a loosened PT structure, ultimately leading to failure of oocyte activation.

Material and methods

Study participants

We recruited 54 infertile couples at the Reproductive and Genetic Hospital of CITIC-Xiangya from January 2014 to June 2020. All

[1]Institute of Reproductive and Stem Cell Engineering, School of Basic Medical Science, Central South University, Changsha 410078, China; [2]Reproductive and Genetic Hospital of CITIC-XIANGYA, Changsha 410078, China; [3]Clinical Research Center for Reproduction and Genetics in Hunan Province, Changsha 410078, China; [4]Hunan Normal University, Changsha 410013, China; [5]Laboratory of Reproductive and Stem Cell Engineering, National Health and Family Planning Commission, Changsha 410078, China
[6]These authors contributed equally
*Correspondence: ustczw@163.com (W.Z.), linggf@hotmail.com (G.L.)
https://doi.org/10.1016/j.ajhg.2021.02.004.

blood and semen samples collected from the affected individuals and control individuals were donated for investigation after the individuals provided informed consent. This present genetic study was approved by the Ethics Committee of the Reproductive and Genetic Hospital of CITIC-Xiangya (reference LL-SC-2017-009).

The inclusion criterion was infertile couples with no fertilization or poor fertilization (defined as a fertilization rate of <20%) who underwent at least one ICSI cycle. The exclusion criterion was infertile couples with less than five metaphase II (MII) oocytes from female individuals and globozoospermic sperm (round-headed sperm that lack acrosomes) from male individuals. The control individuals included 100 male individuals with proven fertility and at least one child.

Mouse oocyte activation test (MOAT)

The verification of male factors in TFF was detected by the MOAT as previously described.[24,25] The MOAT involved injecting sperm from each individual into 30 mouse MII oocytes while simultaneously using sperm from donors with proven fertility as a positive control. Injection was performed as previously described.[26] We assessed the results at around 30 h post-injection by examining the percentage of two-cell formation (number of two-cells versus the number of surviving injected oocytes). The male factors were likely to be the cause of TFF if the percentage of two-cells was less than 20%, while the positive controls should show >90% two-cell formation.

WES and genetic analysis

To identify pathogenic variants of infertile male individuals, we subjected peripheral blood samples to WES by using the following criteria: (1) variants with minor allelic frequencies less than 1% in the gnomAD, 1000 Genomes Project, and Exome Aggregation Consortium databases; (2) exonic non-synonymous or splice-site variants or coding INDELs; (3) homozygous variants or compound-heterozygous variants; and (4) proteins that were abundantly expressed or specifically expressed in human testicular tissue. We assessed functional prediction by using the SIFT and MutationTaster programs. Evolutionary conservation analysis was performed via MultiAlin software. We analyzed protein domains by using the Simple Modular Architecture Research Tool (SMART).

Transmission electron microscopy (TEM)

Sperm from the affected individual and mice were fixed in 2.5% glutaraldehyde (Sigma-Aldrich, G5882) overnight at 4°C. The samples were immersed in 1% osmium tetroxide, dehydrated with graded concentrations of ethanol, and embedded in Epon812, dodecenylsuccinic anhydride, methylnadic anhydride, and dimethylaminomethyl phenol. Ultrathin, 70- to 90-nm-thick sections underwent contrast staining with uranyl acetate and lead citrate, and we examined them by using a Tecnai G2 Spirit TWIN transmission electron microscope (Tecnai) with a Gatan CCD camera (Orius) system.

Real-time quantitative PCR

Total RNA samples were extracted from the peritumoral tissues of donors with cancer after providing informed consent. We synthesized the cDNAs with 1 ug of total RNA by using the PrimeScript RT Reagent Kit. We performed real-time PCR by using a LightCycler 480 II System (Roche) with a SYBR green kit (Roche, 42352720). *GAPDH* (MIM: 138400) was used as an internal control. *ACTL9* mRNA expression was quantified according to the $2^{-\Delta\Delta Ct}$ method. All primers used for real-time PCR are listed in Table S1.

Immunofluorescence staining

Sperm from affected individuals and mice were fixed with 4% paraformaldehyde (Sangon Biotech, E672002) for 30 min at room temperature and then were subjected to permeabilization with 1% Triton X-100 (Sigma, T8787) for 15 min. After being washed with PBS buffer (Sangon Biotech, E607008), we incubated the samples by using blocking buffer containing 5% donkey serum albumin (Jackson ImmunoResearch, 017-000-121) and 2% BSA at 4°C overnight. After staining with goat polyclonal anti-ACTL9 antibody (1:500 dilution; synthesized by YouKe Biotechnology [immunogen: 1–174 amino acids], China), rabbit polyclonal anti-ACTL7A antibody (1:50 dilution; Proteintech, 17355-1-AP), rabbit polyclonal anti-PLCZ1 antibody (1:100 dilution; Abcam, ab124446), donkey anti-rabbit IgG (H+L) highly cross-adsorbed secondary antibody (1:1,000 dilution; Alexa Fluor 594, Invitrogen, A32754), and donkey anti-goat IgG (H+L) cross-adsorbed secondary antibody (1:1,000 dilution; Alexa Fluor 647, Invitrogen, A21447), the sperm were counterstained with fluorescein isothiocyanate-conjugated peanut agglutinin (FITC-PNA, 1:100 dilution; Cellpro Biotech, 09000332405) and 4′, 6′-diamidino-2-phenylindole (DAPI, Sigma, D8417). We used the Celldiscoverer 7 Fluorescence microscope (Zeiss) and Zen 2 software to photograph fluorescence signals and generate line-intensity profiles. We evaluated at least 200 cells in three replicates.

Construction of expression plasmids and transfection

We constructed plasmids encoding wild-type (WT) *ACTL9*/*ACTL7A* (pENTER-*ACTL9*^{His}/pENTER-*ACTL7A*^{cMYC}) and mutant *ACTL9* (pENTER-*ACTL9*^{His}-p.Ser345Leu/Val380Leu/Tyr430Ter). HEK293T cells were cultured to a density at 70%–80% in DMEM (GIBCO, 11965092) with 10% fetal bovine serum (Hyclone, SH30070). We then performed transient transfections by using Lipofectamine 3000 in accordance with the manufacturer's protocol (Thermo Fisher Scientific, L3000015).

Co-immunoprecipitation (co-IP)

To evaluate the interaction between ACTL9 and ACTL7A, we co-transfected WT and mutant *ACTL9* with *ACTL7A* into HEK293T cells. After culturing for 48 h, proteins were isolated from harvested cells lysed in NP-40 Lysis Buffer (Beyotime, P0013F) supplemented with 1 mM PMSF (Beyotime, ST505). Subsequently, proteins were incubated with protein A/G magnetic beads (Thermo Fisher Scientific, 88802) that were cross-linked by a His-tag monoclonal antibody (Proteintech, 66005-1-lg) under gentle rotation at 4°C for 4 h. After washing with lysis buffer three times, the captured protein complexes were eluted with SDT buffer (4% [w/v] SDS and 100 mM Tris/HCl [pH 7.4]) and then denatured with boiling beads for 5 min. Finally, we detected co-IP protein complexes via immunoblotting analysis by using specific antibodies.

Ca^{2+} monitoring

Immature oocytes from donors were obtained after the individuals provided informed consent. The selection conditions for *in vitro*-matured MII oocytes from donors were described in a previous study.[27] *In vitro*-matured MII oocytes were injected with sperm from II-2 in family 1 or a donor and then pre-incubated for 30 min at 37°C in G-MOPS PLUS medium (Vitrolife, 10130) containing the Ca^{2+}-sensitive fluorescent dye Fluo-3 AM (Beyotime, S1056). After ICSI, we transferred the oocytes to G-MOPS PLUS medium for Ca^{2+} analysis. The fluorescence dynamic imaging

via the Celldiscoverer 7 Fluorescence microscope (Zeiss) was subsequently performed every 5 s for a duration of 3 h to capture the fluorescence intensity of intracellular Ca^{2+} oscillations. After Ca^{2+} monitoring, oocytes were fixed at 4 h post-injection, and the expression and localization of PLCζ were evaluated by immunofluorescence staining.

Generation of an *Actl9*-mutated mouse model

We generated an *Actl9*-mutated mouse model carrying the equivalent variant to that in II-1 in family 2 by using CRISPR/Cas9 technology. In brief, Cas9 mRNA, the single-stranded oligonucleotides (ssODNs), and the target of single-guide RNAs (Table S2) were pooled and injected into zygotes from C57BL/6J mice. The genotypes of our knockin mice were validated by PCR with specific primers (Table S3). Six different WT male mice and *Actl9*-mutated male mice were used in the experiments. This study was carried out in accordance with the recommendations of the *Guide for the Care and Use of Laboratory Animals* of the National Institutes of Health, USA.

ICSI in mice

The cauda epididymides were isolated from WT and *Actl9*-mutated male mice (8 weeks old). We released and selected the sperm by using the swim-up method. Oocytes from C57BL/6J female mice (3–6 weeks old) were separately transferred to M2 medium (Sigma, M7167). The polar body of each oocyte was rotated with an injection pipette to the 6 or 12 o'clock position on the modified holding pipette. Mouse oocyte ICSI manipulation was performed as previously described.[28]

ICSI-assisted oocyte activation (AOA) for *ACTL9* variation-associated infertile individuals

ICSI with AOA by calcium ionophore exposure was performed in couples with *ACTL9* variants. For the partner of II-2 in family 1, we performed ovarian stimulation by using an ultra-long protocol and initiated with 187.5 IU of human menopausal gonadotropin (HMG, Livzon). We then triggered final follicular maturation by using 5,000 IU of human chorionic gonadotropin (HCG, Livzon). For the partner of II-2 in family 3, ovarian stimulation was performed with an antagonist protocol and dual-triggered with 0.2 mg of gonadotropin-releasing hormone agonist (GnRHa, IPSEN) and 10,000 IU of HCG. Oocyte retrieval was performed 36 h after HCG injection. Individual sperm were injected singly into mature oocytes followed immediately by exposure to a solution of 10 uM A23187 (Sigma, C9275) for 5 min. Oocytes were extensively washed. Embryos were cultured in 6% CO_2, 5% O_2, and 89% N_2 at 37°C in a humidified incubator. We monitored the fertilization and embryonic development by using time-lapse videography.

Statistical analysis

Data are presented as the mean ± standard error of the mean (SEM). We analyzed our data by using two-tailed Student's t test. A p value of less than 0.05 was considered statistically significant.

Results

Identification of homozygous pathogenic variants in *ACTL9*

To investigate male genetic factors responsible for TFF and poor fertilization, we first identified 21 couples with the male factors from 54 couples suffering from TFF or poor fertilization by MOAT. Then we performed WES analysis on these 21 male individuals. According to our filtering criteria (see material and methods), we identified three of 21 individuals as carrying homozygous pathogenic variants in *PLCZ1* that were previously reported.[17] In addition, we identified homozygous variants in *ACTL9* (GenBank: NM_178525.5) in another three families (Figure 1A), indicating that this was the most likely candidate gene causing TFF. A summary of WES data from the three affected individuals is listed in Table S4. II-2 in family 1 from a consanguineous family had a homozygous missense variant c.1034C>T (p.Ser345Leu). Subsequently, II-1 in family 2 had a homozygous missense variant c.1138G>T (p.Val380Leu) and II-2 in family 3 had a homozygous nonsense variant c.1209C>G (p.Tyr403Ter). These variants were validated by Sanger sequencing (Figure 1A and Table S5). The inheritance pattern in family 2 was uncertain because of the unavailability of DNA samples from the proband's father, whereas families 1 and 3 followed a recessive inheritance pattern. The allelic frequencies of all three variants in gnomAD and ExAC browser are listed in Table 1. The altered amino acid residues were highly conserved across species (Figure 1B). All of the *ACTL9* variants were absent in our control database of 100 male individuals with normal fertility. These findings indicate a possible genetic contribution of *ACTL9* to the TFF phenotype.

Abnormal PT in sperm and TFF in ICSI attempts

The clinical characteristics of three affected individuals with *ACTL9* homozygous variants are listed in Table 2. The percentages of two-cells in the MOAT for all three individuals were 0.0% (Table 2), and the percentage of two-cell formation observed in positive controls was 92.7% ± 1.8%. Proband II-2 in family 1 was a 29-year-old man with a 2-year history of primary infertility. A total of 20 oocytes were retrieved from his partner and fifteen of them were MII oocytes. However, they all failed to extrude a second polar body (PB2), and none of the oocytes were fertilized after separate IVF and ICSI attempts (Figure 2A). Proband II-1 in family 2 was 32 years old with an 8-year history of primary infertility. Six MII oocytes from his partner were injected with sperm of II-1 in family 2 but failed to fertilize and extrude PB2 (Figure 2A). Proband II-2 in family 3 was 33 years old with an 8-year history of primary infertility. His partner suffered from TFF or poor fertilization with three IVF and ICSI attempts, in which a total 45 oocytes were retrieved, and only three of 42 MII oocytes exhibited 2PN after ICSI. These phenomena imply that the failure of fertilization was caused by oocyte activation deficiency.

Sperm morphological study was conducted by hematoxylin and eosin (H&E) staining and TEM. Unlike normal morphology in most reported *PLCZ1*-mutated individuals,[15,17,19] three *ACTL9*-mutated individuals exhibited 2.5%, 2.3%, and 3.2% normal sperm (Table S6), which were all below the reference limit (4%) according to the WHO Standards, Fifth Edition.[29] In addition, these three

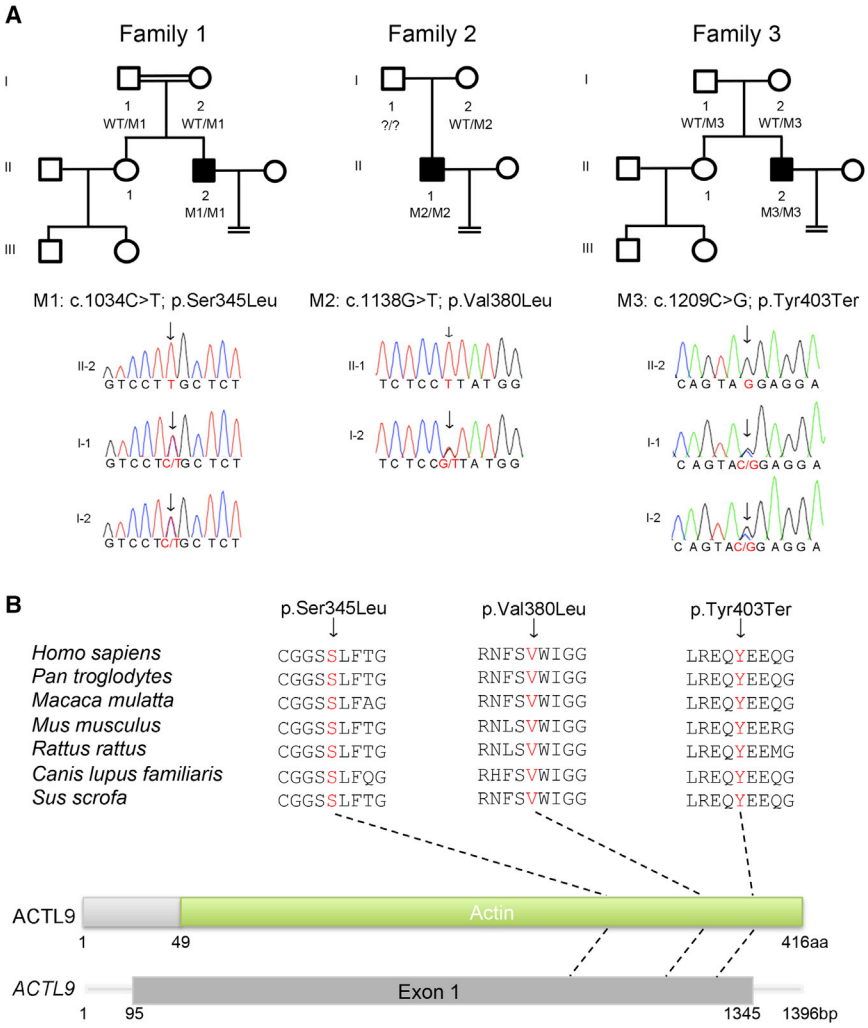

Figure 1. Pedigree-based identification of pathogenic variants in *ACTL9*

(A) Pedigree analysis of three families who experienced TFF or poor fertilization. All three individuals (black squares) exhibited homozygous variants in *ACTL9*; confirmations by Sanger sequencing are shown below the pedigrees. The locations of *ACTL9* variants are depicted in the chromatograms (black arrows).

(B) The variants in localization and conservation of mutant amino acids in ACTL9. All three residues were highly conserved in seven species.

individuals had a high proportion of anomalies in sperm heads, particularly in an increased proportion of tapered-head sperm (11.8%, 14.9%, and 28.5% in three individuals compared to <3% in fertile individuals[30]) (Figure 2B and Table S6). In order to understand the defects observed in the sperm heads of affected individuals, we analyzed ultrastructural aspects of the sperm from II-2 in family 1 by using TEM. Compared with normal controls, we observed mutant sperm to have a loosened PT with a ruffled acrosome, in which the inner acrosomal membrane was detached from the nuclear envelope (Figure 2C). The maximum thickness of the PT was significantly increased in sperm from II-2 in family 1 (290.7 ± 155.6 nm) compared with normal sperm (29.8 ± 6.6 nm) (Figure 2D). This evidence indicates that sperm carrying homozygous pathogenic variants in *ACTL9* lead to abnormal ultrastructure of the PT.

Loss of ACTL9 expression in the equatorial segment of the head region in mutant sperm

First, we analyzed the expression pattern of *ACTL9* in each human adult tissue and found that *ACTL9* was only abundantly expressed in the testis in the GTEx database. This was confirmed by real-time PCR (Figure 3A). In addition, in normally capacitated sperm, ACTL9 was principally localized in the equatorial segment of the head (84.4% ± 11.1%) and neck regions (100.0% ± 0.0%), and a low proportion of sperm exhibited ACTL9 in the acrosomal segment of the head (11.6% ± 10.7%) (Figures 3B and 3C). None of the sperm exhibited a signal with the variants p.Ser345Leu, p.Val380Leu, or p.Tyr403Ter in the equatorial segment of the sperm head. However, the signal in the neck region showed no difference relative to normal controls (Figures 3B and 3C). These results indicate that localization of ACTL9 in the equatorial segment of the head region allows for normal functioning.

Mutant ACTL9 causes a loss of the interaction with ACTL7A necessary to maintain acrosomal anchoring

ACTL7A is known to be the paralog of *ACTL9*. *ACTL7A* is also localized in the subacrosomal layer of the PT and is required to maintain the acrosome ultrastructure.[31] In our study, we performed immunostaining of both ACTL9 and ACTL7A and used the signals from peanut agglutinin (PNA) and DAPI to more closely examine their precise locations by using line-intensity profiles. We found that the ACTL9 signal overlapped almost completely with ACTL7A in the acrosomal or equatorial segments of normal sperm (Figure 3B). Intensity profiles of the acrosomal signal implied that ACTL9 and ACTL7A were co-localized in the subacrosomal layer of the PT that links the acrosome (PNA-positive) to the nuclear envelope (DAPI-positive) (Figure 3B). In addition, intensity profiles of the equatorial signal suggested that ACTL9 and ACTL7A were co-localized in the outer peri-acrosomal layer of the PT and exhibited a strong signal in

Table 1. Overview of the *ACTL9* pathogenic variants observed in the three families

Probands in families	Genomic position on chr19 (bp)	cDNA	Protein	Mutation type	SIFT[a]	MutTas[a]	gnomAD_EAS[b]	ExAC_EAS[b]
Family 1	8808018	c.1034C>T	p.Ser345Leu	missense	D	D	5.4×10^{-5}	N/A
Family 2	8807914	c.1138G>T	p.Val380Leu	missense	D	D	5.4×10^{-5}	0.0001
Family 3	8807843	c.1209C>G	p.Tyr403Ter	nonsense	N/A	D	N/A	N/A

D, damaged; N/A, not available.
[a]Mutation assessment by SIFT and MutationTaster (MutTas).
[b]Allelic frequency of corresponding mutations in the East Asian population according to the gnomAD and ExAC browser.

the outer layer of the nuclear envelope (Figure 3B). These phenomena indicate that ACTL9 together with ACTL7A are located in the PT to participate in normal acrosomal anchoring. In contrast, the ACTL9 signal did not overlap with ACTL7A in mutant sperm. Intensity profiles of the equatorial signal suggested that none of the mutant sperm manifested a strong signal in the equatorial segment (Figure 3B). The acrosome in mutant sperm showed no cap structure. Sperm with the variants p.Ser345Leu and p.Val380Leu exhibited a strong signal in the anterior of the acrosome (Figure 3B). Furthermore, a co-IP assay confirmed that WT ACTL9 indeed combined with ACTL7A, while the interaction was weakened in the variants p.Ser345Leu and p.Val380Leu and was entirely lost in the variant p.Tyr403Ter (Figure 3D). These findings imply that mutant ACTL9 does not interact with ACTL7A, thus leading to abnormal ultrastructure of the PT and defects in acrosomal anchoring.

ACTL9-mutated sperm show PLCζ absence or abnormal localization in the neck region

To understand the relationship between abnormal ultrastructure of the PT and TFF, we investigated the status of PLCζ, a key oocyte activation factor located in the PT.[20,21] Immunostaining showed that the PLCζ signal overlapped with ACTL9 in the equatorial segment of the head of normally capacitated sperm (Figure 4B). However, the proportion of sperm showing no PLCζ signal in mutant capacitated sperm was higher (52.6% ± 0.3% of sperm with the variant p.Ser345Leu, 38.9% ± 9.3% of sperm with the variant p.Val380Leu, and 32.9% ± 1.8% of sperm with the variant p.Tyr403Ter) than normal sperm (18.0% ± 0.6%) (Figure 4A). Moreover, 47.4% ± 0.3% of sperm with the variant p.Ser345Leu, 61.1% ± 9.3% of sperm with the variant p.Val380Leu, and 67.1% ± 1.8% of sperm with the variant p.Tyr403Ter exhibited PLCζ signals in the neck region (Figure 4A), whereas none of the normal sperm exhibited PLCζ signals in the neck region. These results indicate that pathogenic variants in *ACTL9* lead to absence or abnormal localization of PLCζ.

ACTL9-mutated sperm fail to stimulate Ca^{2+} oscillations

To further investigate the activating capacity of mutant sperm, oocytes from donors were injected with mutant or normal sperm to monitor Ca^{2+} oscillations. We monitored 4–5 Ca^{2+} spikes 3 h post-injection in normal controls, but the spikes were absent when we used mutant sperm with the variant p.Ser345Leu (Figure 4C). After monitoring Ca^{2+} oscillations, we fixed oocytes injected with mutant or normal sperm at 4 h post-injection to evaluate the status of PLCζ and observed that PLCζ diffused into the ooplasm in normal fertilized oocytes and these oocytes exited MII arrest. Meanwhile, the sperm asters formed to emit the microtubule structures around the sperm nucleus (Figure 4D).[32] However, one oocyte injected with mutant sperm showed that PLCζ was retained near the sperm head and failed to form the sperm aster (Figure 4D), while the other two oocytes exhibited no PLCζ signals in either ooplasm or the region near the sperm nucleus. These results indicate that the absence or abnormal localization of PLCζ leads to a failure to evoke Ca^{2+} oscillations and oocyte activation.

Sperm from *Actl9*-mutated male mice resembled abnormal ultrastructure of the PT and TFF after ICSI

To investigate whether *ACTL9* pathogenic variants constituted the primary cause of TFF and poor fertilization, we generated the equivalent pathogenic variant noted in II-1 of family 2 in a knockin mouse model. We found that testicular size, testis-to-body-weight ratio, sperm concentration, sperm viability, and sperm motility of sperm in homozygous *Actl9*-mutated male mice ($Actl9^{Mut/Mut}$) showed no significant differences with respect to WT mice (Figures S1A–S1F). Histological examination of the testis and epididymis revealed that the components in the seminiferous epithelium and sperm number in the caudal epididymis of $Actl9^{Mut/Mut}$ mice were similar to those of WT mice (Figures S2A and S2B).

We investigated the morphology of sperm in $Actl9^{Mut/Mut}$ mice by light microscopy and TEM. H&E staining showed that the proportion of sperm without the normal sickle-shaped head in $Actl9^{Mut/Mut}$ mice was higher than in WT, but there was no significant difference (Figures S3A and S3B). TEM showed a loosened PT structure where the acrosome was detached from the nuclear envelope in $Actl9^{Mut/Mut}$ mice sperm, consistent with mutant sperm in humans (Figure 5A). To further investigate the abnormalities in the spermiogenesis that might lead to defects in the PT structure, we performed TEM analysis on the testicular tissue. Compared with normal acrosomal biogenesis,

Table 2. Clinical characteristics of IVF and ICSI attempts in affected individuals

Individual	Previous IVF and ICSI cycles						ICSI with AOA cycles						MOAT[a]
	Insemination method	Total no. of oocytes	No. of mature oocytes	Total fertilization rate	Normal fertilization rate	Good quality embryo rate	Insemination method	Total no. of oocytes	No. of mature oocytes	Total fertilization rate	Normal fertilization rate	Good quality embryo rate	
II-2 in family 1	IVF	6	4	0.0% (0/4)	0.0% (0/4)	– (0/0)	ICSI+AOA	17	14 (7-cryo[b])	100.0% (7/7)	100.0% (7/7)	85.7% (6/7)	0.0% (0/25)[c]
	ICSI	14	11	0.0% (0/11)	0.0% (0/11)	– (0/0)							
II-1 in family 2	ICSI	12	10 (4-cryo[b])	0.0% (0/6)	0.0% (0/6)	– (0/0)	ICSI with donor sperm	14	11	81.8% (9/11)	63.6% (7/11)	28.6% (2/7)	0.0% (0/24)[c]
II-2 in family 3	IVF	11	11	0.0% (0/11)	0.0% (0/11)	– (0/0)	ICSI+AOA	11	8 (4-cryo[b])	100.0% (4/4)	100.0% (4/4)	75.0% (3/4)	0.0% (0/22)[c]
	ICSI	20	19	5.2% (1/19)	5.2% (1/19)	0.0% (0/1)							
	ICSI	14	12	16.7% (2/12)	16.7% (2/12)	100.0% (2/2)							

[a]MOAT represents mouse oocyte activation test.
[b]Number of mature oocytes cryopreserved.
[c]Number of two-cells versus the number of surviving injected oocytes in the MOAT.

we found that proacrosomal vesicles in the Golgi phase were atypical and separated in the testis of *Actl9*$^{Mut/Mut}$ mice (Figure 5B). We also observed failed fusion of additional proacrosomal vesicles in the cap phase (Figure 5B). These phenomena indicate that spermatids carrying the *Actl9* pathogenic variant lead to defects in the fusion of proacrosomal vesicles that result in ruffled acrosomes with a loosened PT formed in mature sperm.

To examine the fertilization ability of sperm from *Actl9*$^{Mut/Mut}$ in mice, we performed ICSI in these mice and found that none of the oocytes fertilized successfully (Figures 5C–5E). Thus, our results in *Actl9*-mutated mice resembled the TFF phenotype in humans, indicating that the original variant was a likely infertility driver in male individuals.

Rescue of the *ACTL9* defect by ICSI with AOA

Our previous study revealed that *PLCZ1* variation-associated TFF was rescued by ICSI with AOA.[17] Because *ACTL9*-mutated sperm failed to induce Ca^{2+} oscillations in oocytes, we explored whether the infertility caused by pathogenic variants in *ACTL9* could be rescued via ICSI with AOA by Ca^{2+} ionophore exposure. II-2 in family 1 and family 3 volunteered to attempt this method and signed the informed consent. After mutation screening for the partner to exclude rare variants in *ACTL9,* oocytes were injected with sperm from the affected individuals. All oocytes achieved successful normal fertilization, and 85.7% and 75.0% of the derived zygotes developed into good-quality embryos in II-2 in family 1 and II-2 in family 3, respectively (Table 2). We monitored the fertilization and embryonic development of II-2 in family 1 by using time-lapse videography (Video S1). After embryo selection, we transferred embryos (one eight-cell embryo and one seven-cell embryo) on day 3 and achieved pregnancies, and two healthy babies were born in family 1. Family 3 chose to cryopreserve embryos, which have not yet been transplanted. These results suggest that *ACTL9* variation-associated infertility could be successfully overcome with ICSI with AOA.

Discussion

In many cases of infertility, the causes of TFF remain unclear and cannot be determined on the basis of available morphological data. For a considerable period of time, *PLCZ1* was the only reported sperm-borne factor to cause TFF, excluding globozoospermia, in individuals.[14–19] Recently, *ACTL7A* was added as another male factor associated with TFF due to reduced expression and abnormal localization of PLCζ.[23] In the present study, we investigated 21 male individuals who underwent at least one ICSI cycle without successful fertilization and identified

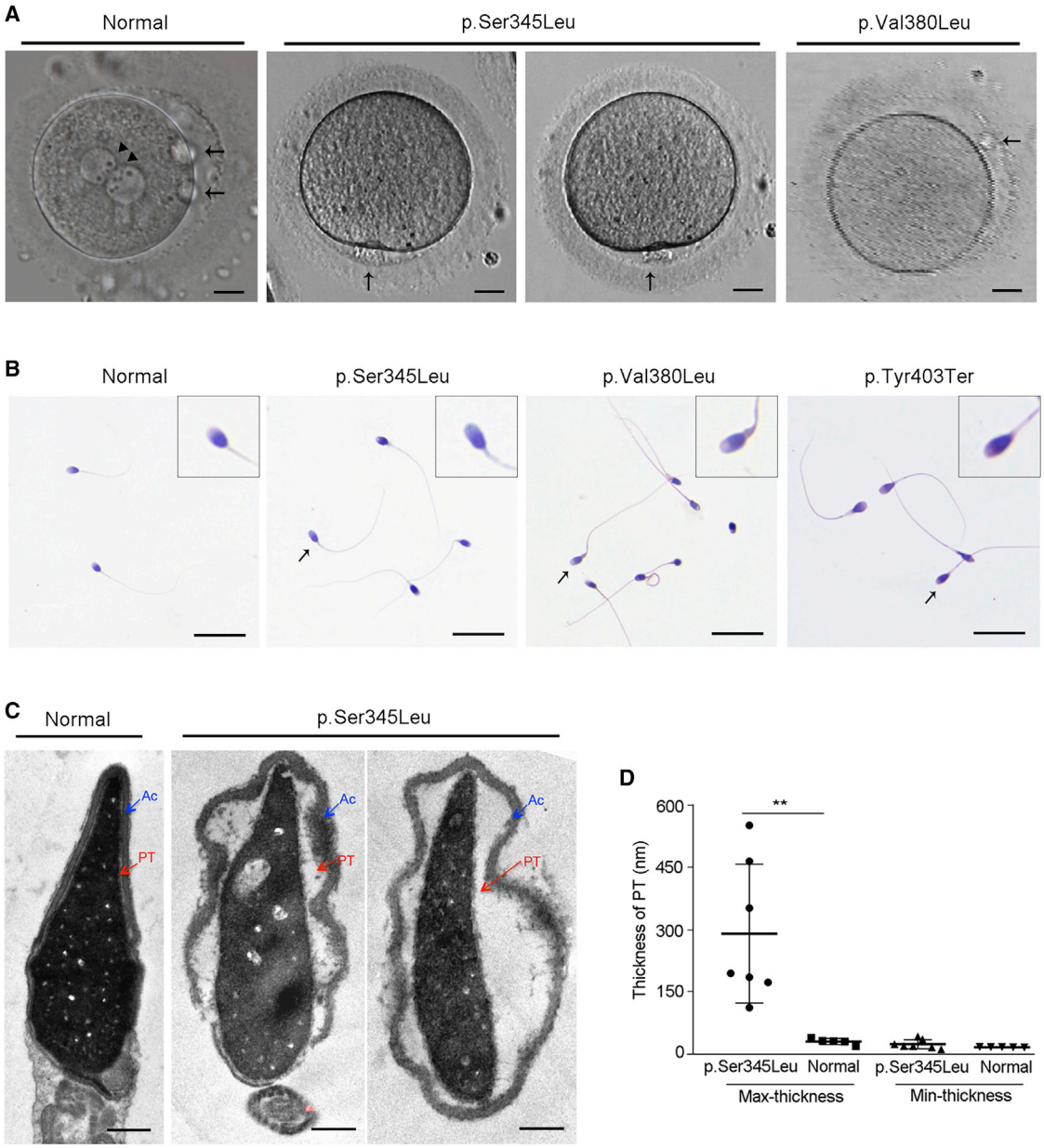

Figure 2. Affected individuals with *ACTL9* pathogenic variants exhibited TFF and ruffled acrosome phenotypes

(A) Unfertilized oocytes injected with *ACTL9*-mutated sperm at 15–18 h post-injection. Extrusion of PB2 was not observed in the unfertilized oocytes (black arrowhead). In normal fertilized oocytes, we observed two pronuclei (black triangle) and two polar bodies (black arrowhead). Scale bars, 20 μm.

(B) Light microscopy analysis of sperm from a normal donor and individuals with *ACTL9* pathogenic variants. Black triangle represents normal sperm. Black arrowheads represent tapered-head sperm with increased major axis length and normal minor axis length. The magnified panel at the upper right corner shows views of heads. Scale bars, 20 μm.

(C) Ultrastructure of sperm from a normal donor and an affected individual. In normal sperm, the acrosome (Ac, blue arrowhead) was extended as a dense cap-shaped structure covering the nucleus. The perinuclear theca (PT, red arrowhead) is shown fastening the developed acrosome to the nuclear membrane. In sperm with the p.Ser345Leu variant, the acrosome was detached from the nucleus, with an irregular PT. Scale bars, 0.5 μm.

(D) The thickness of the PT in sperm from donors and an affected individual. Max-thickness represents the maximum thickness of the PT. Min-thickness represents the minimum thickness of the PT. **$p < 0.01$.

three homozygous pathogenic variants in *ACTL9* impacting the ultrastructure of the PT, ultimately leading to absent or abnormal localization of PLCζ with subsequent oocyte activation failure and TFF.

The PT is a structure that fastens the developing acrosome to the nuclear membrane.[22] The biogenesis of the PT is accompanied with acrosomal biogenesis, which is a continuous process that takes place throughout the reproductive lifespan of the male. Proacrosomal vesicles are derived from the trans-Golgi network of the Golgi apparatus and fuse into an acrosomal sac that associates with the nuclear envelope via the PT.[33] Fusion of

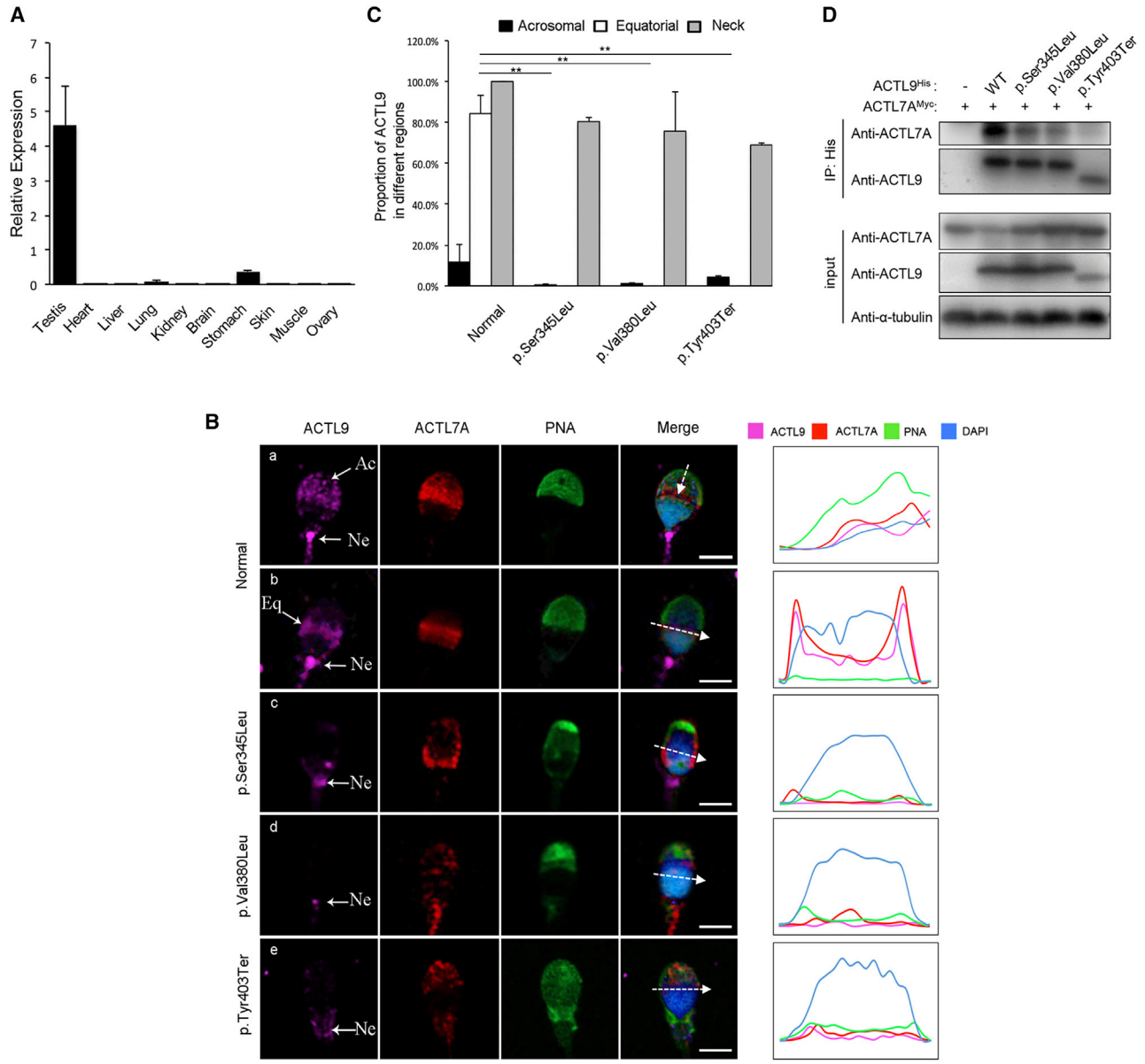

Figure 3. Mutant testis-specific protein ACTL9 is absent from the equatorial segment and not co-localized with ACTL7A

(A) The relative expression of *ACTL9* mRNA in ten human tissues. Bars indicate means ± SEM.

(B) Immunostaining of ACTL9 and ACTL7A in sperm from donors and affected individuals. In normal sperm, ACTL9 (pink) is localized to the acrosomal, equatorial segment of the head and neck regions (a and b). ACTL7A (red) is shown to overlap with ACTL9 in the sperm head. In sperm with the p.Ser345Leu (c), p.Val380Leu (d), or p.Tyr403Ter (e) variant, ACTL9 is only localized to the neck region. ACTL7A does not overlap with ACTL9. Line-intensity profiles show the precise localization of ACTL9 in the acrosome and equatorial segment. Scale bars, 3 μm.

(C) The proportion of ACTL9 in different regions of sperm from donors and affected individuals. **$p < 0.01$. Bars indicate means ± SEM.

(D) The interaction between ACTL9 and ACTL7A following co-IP in HEK293 cells. Wild-type his-tagged ACTL9 interacts with ACTL7A. This interaction is weakened in the variants p.Ser345Leu and p.Val380Leu and is completely lost in the nonsense variant p.Tyr403Ter, with a shortened band. α-tubulin was used as the internal control.

additional proacrosomal vesicles then continues as the acrosome increases in size to the point where it spreads over the anterior portion of the nucleus.[33] Although the morphogenetic process of the acrosome has been well-studied, the molecular mechanism(s) underlying acrosomal and the PT biogenesis remains unelucidated. In our study, sperm of *Actl9*$^{Mut/Mut}$ mice failed to show fusion of proacrosomal vesicles and displayed ruffled acrosomes with a loosened PT. We consider that this actin-like protein plays an important role in the fusion of proacrosomal vesicles and the PT formation. These results have thus enhanced our understanding of the molecular mechanism governing biogenesis of the acrosome and PT. In addition, unlike the normal morphology in *PLCZ1*-mutated sperm mentioned in the previous studies,[15,17,19] the morphology of *ACTL9*-mutated sperm

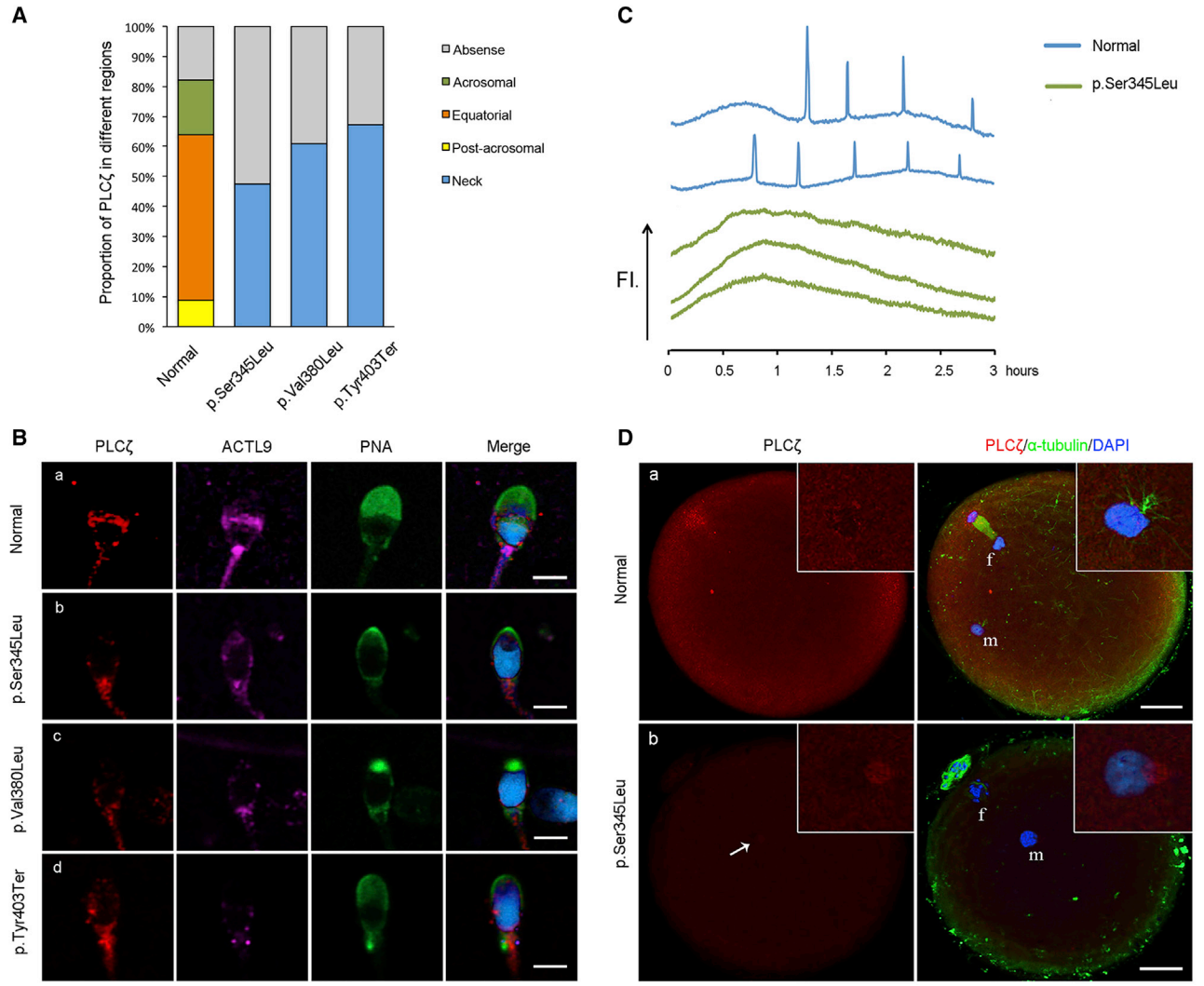

Figure 4. Sperm with *ACTL9* pathogenic variants showing absent or abnormally localized PLCζ failed to trigger Ca^{2+} oscillations
(A) The proportion of PLCζ in different sperm regions from donors and affected individuals.
(B) Immunostaining of PLCζ in sperm from donors and affected individuals. In normal sperm, PLCζ is primarily localized to the equatorial segment of the sperm, overlapping with ACTL9 in the same region (a). In sperm with the variants p.Ser345Leu (b), p.Val380Leu (c), and p.Tyr403Ter (d), PLCζ is localized to the neck region, overlapping with ACTL9 in the neck region. Scale bars, 3 μm.
(C) Profile of Ca^{2+} responses induced by oocyte injection with sperm from donors and an affected individual. Normal sperm induced 4–5 Ca^{2+} spikes in 3 h (blue line), while mutant sperm with the variant p.Ser345Leu failed to induce spikes (green line).
(D) Immunostaining of oocytes injected with sperm from donors and an affected individual. An oocyte injected with normal sperm (a) shows exiting MII arrest (f) with an extruding PB2. Additionally, sperm aster (m) was formed. PLCζ staining is diffused across the ooplasm. An oocyte injected with sperm with the variant p.Ser345Leu remains in MII arrest (f), and PLCζ is retained in a region near the sperm head (m, white arrowhead). The magnified panel at the upper right corner shows views of the sperm nucleus. Scale bars, 20 μm.

exhibited a high proportion of tapered heads. The relationship between tapered-head sperm and *ACTL9* variation needs further investigation.

Our current understanding is that actin-related proteins are often present in pairs or in multimeric protein complexes.[34–36] In the testis, a number of actin-related genes have been reported, including *ACTRT1* (MIM: 300487), *ACTRT2* (MIM: 608535), *ACTRT3* (MIM: 608534), *ACTL7A*, and *ACTL7B* (MIM: 604304).[37–41] *ACTL7A* is an important paralog of *ACTL9*. In our study, the testis-specific actin-like protein ACTL9 was localized to the PT structure and interacted with ACTL7A in sperm. This was also confirmed by *in vitro* experiments. Mutant ACTL9 had weakened or lost interaction with ACTL7A. These findings imply that ACTL9 and ACTL7A may form complexes that participate in the PT formation and acrosomal anchoring. Pathogenic variants in *ACTL9* might cause dysfunction in these complexes, resulting in the inner acrosomal membrane's detaching from the nuclear envelope and forming a loosened PT structure. In addition, *in vitro* experiments proved that the nonsense variant p.Tyr403Ter in ACTL9 lost the ability to interact with ACTL7A. This suggests that the main interaction site may be located in the downstream region of the 403rd amino residue.

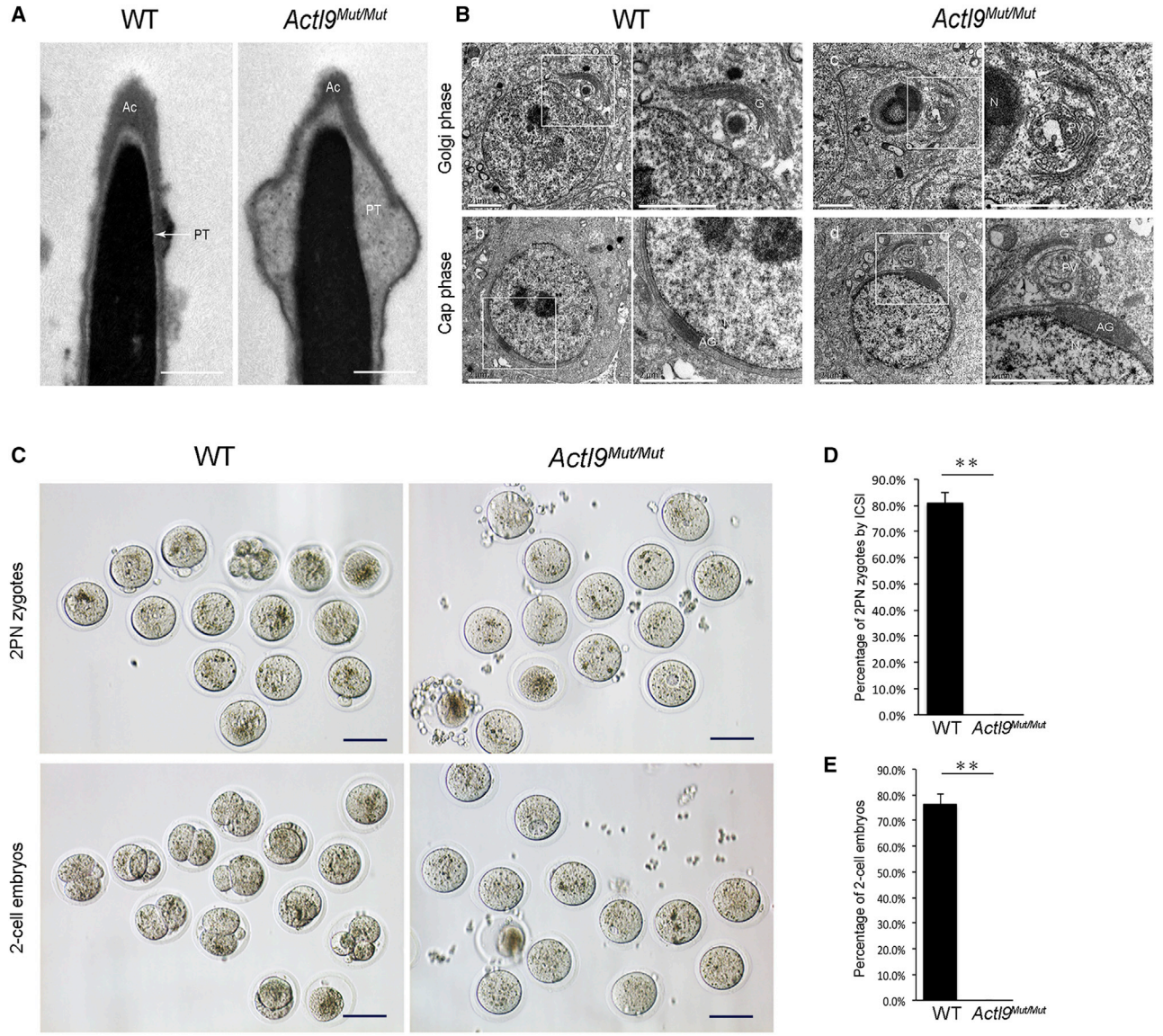

Figure 5. Homozygous *Actl9*-mutated mice show defects in acrosomal biogenesis and sperm that failed to fertilize via ICSI

(A) The ultrastructure of sperm from WT and *Actl9*$^{Mut/Mut}$ mice. Ac represents the acrosome. PT represents the perinuclear theca. Scale bars, 0.5 μm.

(B) Acrosomal biogenesis of WT and *Actl9*$^{Mut/Mut}$ mice. In normal acrosomal biogenesis (a and b), proacrosomal vesicles (PVs) derived from the trans-Golgi network fused into a single acrosomal sac (Golgi phase, a). Acrosomal granules (AGs) that were glycoprotein rich then began to flatten upon touching the nuclear envelope and spread over the nucleus (N) to form a cap (cap phase, b). For *Actl9*$^{Mut/Mut}$ mice (c and d), proacrosomal vesicles in the Golgi phase (c) remained atypical, separated, and failed to fuse into an entire vesicle in the cap phase (d). The magnified panels on the right show perspectives in white squares. *Actl9*$^{Mut/Mut}$ represents male mice with the homozygous pathogenic variant in *Actl9*. Scale bars, 2 μm.

(C) Representative 2PN zygotes and two-cell embryos after ICSI in WT and *Actl9*$^{Mut/Mut}$ mice. Scale bars, 100 μm.

(D) The proportion of 2PN zygotes after ICSI in WT and *Actl9*$^{Mut/Mut}$ mice. No 2PN zygotes were formed from sperm with the *Actl9* pathogenic variant. Bars indicate means ± SEM. **$p < 0.01$.

(E) The proportion of two-cell embryos in WT and *Actl9*$^{Mut/Mut}$ mice. No two-cell embryo was formed from sperm with the *Actl9* pathogenic variant. Bars indicate means ± SEM. **$p < 0.01$.

Many studies have shown that ICSI with sperm with globozoospermia did not lead to successful fertilization because the acrosome was lost and PLCζ failed to be retained in the PT structure.[42,43] The role of the PT has become important during fertilization, particularly in cases with severe teratozoospermia with cephalic abnormalities associated with acrosomal hypoplasia.[44] We detected a loosened PT in this study, however the relationship between a loosened PT and TFF via ICSI remains unknown. We found PLCζ to be absent or abnormally localized to the neck region relative to its location in the head of the normal sperm. We speculate that the loss of PLCζ is caused by the loosened PT structure that is lost with excess cytoplasmic residues during spermatogenesis. A deficiency in PLCζ has been

reported to be associated with a failure of oocyte activation and TFF in humans.[45] Intriguingly, PLCζ still persisted in approximately half of the sperm analyzed but was abnormally located in the neck region. We speculate that the mechanism underlying the neck localization of PLCζ may involve the interaction between ACTL9 and PLCζ. Although the role of neck-localized ACTL9 remains unclear, it might play an important role in the head-neck connection or it might only be part of the cytoplasmic residue. Thus, the specific mechanism(s) involved requires further studies. To investigate the influence of PLCζ in the neck region, we observed that sperm with PLCζ in this region could not diffuse into the ooplasm and failed to induce Ca^{2+} oscillations. These results imply that PLCζ in the neck region may not be efficiently released into the ooplasm, and the specific mechanism involved in this process requires further study.

In a previous study, the condition of male individuals with pathogenic variants in *PLCZ1* and whose sperm failed to trigger Ca^{2+} oscillations in the oocytes was rescued via ICSI with AOA, achieving successful fertilization and pregnancy.[17] In the current study, after mutation screening for the partner, we utilized the most commonly used activating agent, calcium ionophore A23187, to activate oocytes injected with *ACTL9* mutant sperm from two affected individuals. After transferring two good-quality embryos on day 3 to the partner of II-2 in family 1, two healthy babies were born, demonstrating an effective way to overcome the fertilization problem of sperm with homozygous *ACTL9* pathogenic variants. In conclusion, homozygous pathogenic variants in *ACTL9* led to a loosened PT in sperm that failed to fertilize via ICSI in humans and mice. Our study thus provides a basis for the genetic diagnosis of TFF and male infertility and suggests a treatment method for affected individuals.

Data and code availability

The WES datasets supporting the current study are available from the corresponding authors on request. The NCBI reference sequence numbers for human *ACTL9* transcript, ACTL9, and mouse *Actl9* transcript are GenBank: NM_178525.5, NP_848620.3, and NM_183282.2, respectively.

Supplemental Data

Supplemental Data can be found online at https://doi.org/10.1016/j.ajhg.2021.02.004.

Acknowledgments

This work was supported by grants from the National Key Research and Development Program of China (2016YFC1000200); the Science and Technology Major Project of the Ministry of Science and Technology of Hunan Province, China (2017SK1032); the Hunan Provincial Grant for Innovative Province Construction (2019SK4012); and the Scientific Research Foundation of Reproductive and Genetic Hospital of China International Trust Investment Corporation (CITIC) Xiangya (YNXM-201907 and YNXM-201810).

Declaration of interests

The authors declare no competing interests.

Received: September 3, 2020
Accepted: February 2, 2021
Published: February 23, 2021

Web resources

1000 Genomes Project, https://www.internationalgenome.org/home
dbSNP, https://www.ncbi.nlm.nih.gov/projects/SNP/
ExAC browser, http://exac.broadinstitute.org/
GeneBank, https://www.ncbi.nlm.nih.gov/genbank/
gnomAD, https://gnomad.broadinstitute.org/
GTEx, http://gtexportal.org/home/index.html
MultiAlin, http://multalin.toulouse.inra.fr/multalin/multalin.html
MutationTaster, http://www.mutationtaster.org/
OMIM, https://www.omim.org/
SIFT, https://sift.bii.a-star.edu.sg/
SMART, http://smart.embl-heidelberg.de/

References

1. Satouh, Y., and Ikawa, M. (2018). New Insights into the Molecular Events of Mammalian Fertilization. Trends Biochem. Sci. *43*, 818–828.
2. Nomikos, M., Swann, K., and Lai, F.A. (2012). Starting a new life: sperm PLC-zeta mobilizes the Ca2+ signal that induces egg activation and embryo development: an essential phospholipase C with implications for male infertility. BioEssays *34*, 126–134.
3. Saleh, A., Kashir, J., Thanassoulas, A., Safieh-Garabedian, B., Lai, F.A., and Nomikos, M. (2020). Essential Role of Sperm-Specific PLC-Zeta in Egg Activation and Male Factor Infertility: An Update. Front. Cell Dev. Biol. *8*, 28.
4. Mahutte, N.G., and Arici, A. (2003). Failed fertilization: is it predictable? Curr. Opin. Obstet. Gynecol. *15*, 211–218.
5. Kahyaoglu, I., Demir, B., Turkkanı, A., Cınar, O., Dilbaz, S., Dilbaz, B., and Mollamahmutoglu, L. (2014). Total fertilization failure: is it the end of the story? J. Assist. Reprod. Genet. *31*, 1155–1160.
6. Liu, D.Y., and Baker, H.W. (2000). Defective sperm-zona pellucida interaction: a major cause of failure of fertilization in clinical in-vitro fertilization. Hum. Reprod. *15*, 702–708.
7. Rawe, V.Y., Olmedo, S.B., Nodar, F.N., Doncel, G.D., Acosta, A.A., and Vitullo, A.D. (2000). Cytoskeletal organization defects and abortive activation in human oocytes after IVF and ICSI failure. Mol. Hum. Reprod. *6*, 510–516.
8. van der Westerlaken, L., Helmerhorst, F., Dieben, S., and Naaktgeboren, N. (2005). Intracytoplasmic sperm injection as a treatment for unexplained total fertilization failure or low fertilization after conventional in vitro fertilization. Fertil. Steril. *83*, 612–617.

9. Nasr-Esfahani, M.H., Deemeh, M.R., and Tavalaee, M. (2010). Artificial oocyte activation and intracytoplasmic sperm injection. Fertil. Steril. *94*, 520–526.
10. Kashir, J., Heindryckx, B., Jones, C., De Sutter, P., Parrington, J., and Coward, K. (2010). Oocyte activation, phospholipase C zeta and human infertility. Hum. Reprod. Update *16*, 690–703.
11. Sang, Q., Li, B., Kuang, Y., Wang, X., Zhang, Z., Chen, B., Wu, L., Lyu, Q., Fu, Y., Yan, Z., et al. (2018). Homozygous Mutations in WEE2 Cause Fertilization Failure and Female Infertility. Am. J. Hum. Genet. *102*, 649–657.
12. Alazami, A.M., Awad, S.M., Coskun, S., Al-Hassan, S., Hijazi, H., Abdulwahab, F.M., Poizat, C., and Alkuraya, F.S. (2015). TLE6 mutation causes the earliest known human embryonic lethality. Genome Biol. *16*, 240.
13. Chen, B., Wang, W., Peng, X., Jiang, H., Zhang, S., Li, D., Li, B., Fu, J., Kuang, Y., Sun, X., et al. (2019). The comprehensive mutational and phenotypic spectrum of TUBB8 in female infertility. Eur. J. Hum. Genet. *27*, 300–307.
14. Kashir, J., Konstantinidis, M., Jones, C., Lemmon, B., Lee, H.C., Hamer, R., Heindryckx, B., Deane, C.M., De Sutter, P., Fissore, R.A., et al. (2012). A maternally inherited autosomal point mutation in human phospholipase C zeta (PLCζ) leads to male infertility. Hum. Reprod. *27*, 222–231.
15. Escoffier, J., Lee, H.C., Yassine, S., Zouari, R., Martinez, G., Karaouzène, T., Coutton, C., Kherraf, Z.E., Halouani, L., Triki, C., et al. (2016). Homozygous mutation of PLCZ1 leads to defective human oocyte activation and infertility that is not rescued by the WW-binding protein PAWP. Hum. Mol. Genet. *25*, 878–891.
16. Torra-Massana, M., Cornet-Bartolomé, D., Barragán, M., Durban, M., Ferrer-Vaquer, A., Zambelli, F., Rodriguez, A., Oliva, R., and Vassena, R. (2019). Novel phospholipase C zeta 1 mutations associated with fertilization failures after ICSI. Hum. Reprod. *34*, 1494–1504.
17. Dai, J., Dai, C., Guo, J., Zheng, W., Zhang, T., Li, Y., Lu, C., Gong, F., Lu, G., and Lin, G. (2020). Novel homozygous variations in PLCZ1 lead to poor or failed fertilization characterized by abnormal localization patterns of PLCζ in sperm. Clin. Genet. *97*, 347–351.
18. Mu, J., Zhang, Z., Wu, L., Fu, J., Chen, B., Yan, Z., Li, B., Zhou, Z., Wang, W., Zhao, L., et al. (2020). The identification of novel mutations in PLCZ1 responsible for human fertilization failure and a therapeutic intervention by artificial oocyte activation. Mol. Hum. Reprod. *26*, 80–87.
19. Yan, Z., Fan, Y., Wang, F., Yan, Z., Li, M., Ouyang, J., Wu, L., Yin, M., Zhao, J., Kuang, Y., et al. (2020). Novel mutations in PLCZ1 cause male infertility due to fertilization failure or poor fertilization. Hum. Reprod. *35*, 472–481.
20. Fujimoto, S., Yoshida, N., Fukui, T., Amanai, M., Isobe, T., Itagaki, C., Izumi, T., and Perry, A.C. (2004). Mammalian phospholipase Czeta induces oocyte activation from the sperm perinuclear matrix. Dev. Biol. *274*, 370–383.
21. Escoffier, J., Yassine, S., Lee, H.C., Martinez, G., Delaroche, J., Coutton, C., Karaouzène, T., Zouari, R., Metzler-Guillemain, C., Pernet-Gallay, K., et al. (2015). Subcellular localization of phospholipase Cζ in human sperm and its absence in DPY19L2-deficient sperm are consistent with its role in oocyte activation. Mol. Hum. Reprod. *21*, 157–168.
22. Escalier, D. (1990). Failure of differentiation of the nuclear-perinuclear skeletal complex in the round-headed human spermatozoa. Int. J. Dev. Biol. *34*, 287–297.
23. Xin, A., Qu, R., Chen, G., Zhang, L., Chen, J., Tao, C., Fu, J., Tang, J., Ru, Y., Chen, Y., et al. (2020). Disruption in ACTL7A causes acrosomal ultrastructural defects in human and mouse sperm as a novel male factor inducing early embryonic arrest. Sci. Adv. *6*, eaaz4796.
24. Heindryckx, B., Van der Elst, J., De Sutter, P., and Dhont, M. (2005). Treatment option for sperm- or oocyte-related fertilization failure: assisted oocyte activation following diagnostic heterologous ICSI. Hum. Reprod. *20*, 2237–2241.
25. Heindryckx, B., De Gheselle, S., Gerris, J., Dhont, M., and De Sutter, P. (2008). Efficiency of assisted oocyte activation as a solution for failed intracytoplasmic sperm injection. Reprod. Biomed. Online *17*, 662–668.
26. Rybouchkin, A., Dozortsev, D., Pelinck, M.J., De Sutter, P., and Dhont, M. (1996). Analysis of the oocyte activating capacity and chromosomal complement of round-headed human spermatozoa by their injection into mouse oocytes. Hum. Reprod. *11*, 2170–2175.
27. Zhang, S.P., Lu, C.F., Gong, F., Xie, P.Y., Hu, L., Zhang, S.J., Lu, G.X., and Lin, G. (2017). Polar body transfer restores the developmental potential of oocytes to blastocyst stage in a case of repeated embryo fragmentation. J. Assist. Reprod. Genet. *34*, 563–571.
28. Lyu, Q.F., Deng, L., Xue, S.G., Cao, S.F., Liu, X.Y., Jin, W., Wu, L.Q., and Kuang, Y.P. (2010). New technique for mouse oocyte injection via a modified holding pipette. Reprod. Biomed. Online *21*, 663–666.
29. Cooper, T.G., Noonan, E., von Eckardstein, S., Auger, J., Baker, H.W., Behre, H.M., Haugen, T.B., Kruger, T., Wang, C., Mbizvo, M.T., and Vogelsong, K.M. (2010). World Health Organization reference values for human semen characteristics. Hum. Reprod. Update *16*, 231–245.
30. Auger, J., Jouannet, P., and Eustache, F. (2016). Another look at human sperm morphology. Hum. Reprod. *31*, 10–23.
31. Boëda, B., Knowles, P.P., Briggs, D.C., Murray-Rust, J., Soriano, E., Garvalov, B.K., McDonald, N.Q., and Way, M. (2011). Molecular recognition of the Tes LIM2-3 domains by the actin-related protein Arp7A. J. Biol. Chem. *286*, 11543–11554.
32. Terada, Y., Nakamura, S.I., Hewitson, L., Simerly, C., Horiuchi, T., Murakami, T., Okamura, K., and Schatten, G. (2002). Human sperm aster formation after intracytoplasmic sperm injection with rabbit and bovine eggs. Fertil. Steril. *77*, 1283–1284.
33. Khawar, M.B., Gao, H., and Li, W. (2019). Mechanism of Acrosome Biogenesis in Mammals. Front. Cell Dev. Biol. *7*, 195.
34. Goley, E.D., Ohkawa, T., Mancuso, J., Woodruff, J.B., D'Alessio, J.A., Cande, W.Z., Volkman, L.E., and Welch, M.D. (2006). Dynamic nuclear actin assembly by Arp2/3 complex and a baculovirus WASP-like protein. Science *314*, 464–467.
35. Kiselar, J.G., Mahaffy, R., Pollard, T.D., Almo, S.C., and Chance, M.R. (2007). Visualizing Arp2/3 complex activation mediated by binding of ATP and WASp using structural mass spectrometry. Proc. Natl. Acad. Sci. USA *104*, 1552–1557.
36. Chhabra, E.S., and Higgs, H.N. (2007). The many faces of actin: matching assembly factors with cellular structures. Nat. Cell Biol. *9*, 1110–1121.
37. Chadwick, B.P., Mull, J., Helbling, L.A., Gill, S., Leyne, M., Robbins, C.M., Pinkett, H.W., Makalowska, I., Maayan, C., Blumenfeld, A., et al. (1999). Cloning, mapping, and expression of two novel actin genes, actin-like-7A (ACTL7A) and actin-like-7B (ACTL7B), from the familial dysautonomia candidate region on 9q31. Genomics *58*, 302–309.

38. Heid, H., Figge, U., Winter, S., Kuhn, C., Zimbelmann, R., and Franke, W. (2002). Novel actin-related proteins Arp-T1 and Arp-T2 as components of the cytoskeletal calyx of the mammalian sperm head. Exp. Cell Res. *279*, 177–187.
39. Hisano, M., Yamada, S., Tanaka, H., Nishimune, Y., and Nozaki, M. (2003). Genomic structure and promoter activity of the testis haploid germ cell-specific intronless genes, Tact1 and Tact2. Mol. Reprod. Dev. *65*, 148–156.
40. Tanaka, H., Iguchi, N., Egydio de Carvalho, C., Tadokoro, Y., Yomogida, K., and Nishimune, Y. (2003). Novel actin-like proteins T-ACTIN 1 and T-ACTIN 2 are differentially expressed in the cytoplasm and nucleus of mouse haploid germ cells. Biol. Reprod. *69*, 475–482.
41. Hara, Y., Yamagata, K., Oguchi, K., and Baba, T. (2008). Nuclear localization of profilin III-ArpM1 complex in mouse spermiogenesis. FEBS Lett. *582*, 2998–3004.
42. Modarres, P., Tavalaee, M., Ghaedi, K., and Nasr-Esfahani, M.H. (2019). An Overview of The Globozoospermia as A Multigenic Identified Syndrome. Int. J. Fertil. Steril. *12*, 273–277.
43. Tavalaee, M., Nomikos, M., Lai, F.A., and Nasr-Esfahani, M.H. (2018). Expression of sperm PLCζ and clinical outcomes of ICSI-AOA in men affected by globozoospermia due to DPY19L2 deletion. Reprod. Biomed. Online *36*, 348–355.
44. Chemes, E.H., and Rawe, Y.V. (2003). Sperm pathology: a step beyond descriptive morphology. Origin, characterization and fertility potential of abnormal sperm phenotypes in infertile men. Hum. Reprod. Update *9*, 405–428.
45. Yoon, S.Y., Jellerette, T., Salicioni, A.M., Lee, H.C., Yoo, M.S., Coward, K., Parrington, J., Grow, D., Cibelli, J.B., Visconti, P.E., et al. (2008). Human sperm devoid of PLC, zeta 1 fail to induce Ca(2+) release and are unable to initiate the first step of embryo development. J. Clin. Invest. *118*, 3671–3681.